Making a Simple $A + B \to C$ Reaction Oscillate by Coupling to Hydrodynamic Effect

M. A. Budroni,[1,2,*,‡] V. Upadhyay,[1,‡] and L. Rongy[1,†]

[1]*Nonlinear Physical Chemistry Unit, Faculté des Sciences, Université libre de Bruxelles (ULB),*
CP231, 1050 Brussels, Belgium
[2]*Department of Chemistry and Pharmacy, University of Sassari, Via Vienna 2, Sassari 07100, Italy*

We present a new mechanism through which chemical oscillations and waves can be induced in batch conditions with a simple $A + B \to C$ reaction in the absence of any nonlinear chemical feedback or external trigger. Two reactants A and B, initially separated in space, react upon diffusive contact and the product actively fuels *in situ* convective Marangoni flows by locally increasing the surface tension at the mixing interface. These flows combine in turn with the reaction-diffusion dynamics, inducing damped spatiotemporal oscillations of the chemical concentrations and the velocity field. By means of numerical simulations, we single out the detailed mechanism and minimal conditions for the onset of this periodic behavior. We show how the antagonistic coupling with buoyancy convection, due to concurrent chemically induced density changes, can control the oscillation properties, sustaining or suppressing this phenomenon depending on the relative strength of buoyancy- and surface-tension-driven forces. The oscillatory instability is characterized in the relevant parametric space spanned by the reactor height, the Marangoni (Ma_i) and the Rayleigh (Ra_i) numbers of the ith chemical species, the latter ruling the surface tension and buoyancy contributions to convection, respectively.

The design and control of self-organized functional behaviors represent challenging targets in complexity. While many approaches rely on external stimuli to drive the dynamics of responsive systems [1,2], chemical reactions provide an internal pathway to promote emergent behaviors by changing *in situ* the chemophysical properties of a reactive medium. In particular, oscillating reactions are among the most interesting model systems where self-sustained patterns can be chemically controlled [3,4]. Chemical oscillations are currently explored within bottom-up frameworks for understanding biological functionalities as complex as morphogenesis, cellular communication, synchronization, and quorum sensing phenomena [5–7]. Chemical oscillators are also studied for building chemical artificial intelligence [8,9] and controlling hydrogen production [10], exploited in the realm of materials science for designing mechanically responsive materials [11], self-propelled motion [12], or smart drug delivery strategies [13].

Over the last three decades, the innermost mechanisms for spontaneous chemical oscillations and waves have been elucidated from a chemical perspective, showing the need of nonlinear chemical steps activated on appropriate relative timescales [14]. The whole landscape of reactions that meet the necessary constraints is, however, a very restricted family.

In this context, we present a chemophysical mechanism through which spontaneous chemical spatiotemporal oscillations can emerge in batch conditions with a simple $A + B \to C$ reaction, in the absence of any kinetic feedback. To this aim, we use the classical system where two reactants A and B are initially separated in space and start to react upon diffusive contact (see Fig. 1), following a bimolecular kinetics [15]. The interplay between the chemical kinetics and diffusion creates a reaction front, i.e., a localized region with nonzero production rate, whose reaction-diffusion (RD) structural and dynamical properties have been extensively analyzed [15,16]. The onset of chemically driven convection [17], due to local changes in the properties of the medium (e.g., density, surface tension, viscosity), can feedback on such RD structures and provide a new variety of reaction-diffusion-convection (RDC) dynamics [18–20]. Their control is at the heart of several applied problems as diverse as extraction [21], CO_2 sequestration techniques [22,23], crystal growth [24], atmospheric chemistry [25], and contaminant remediation [26].

Most previous works on reactive flows triggered by an active RDC coupling focused either on the impact of chemical reactions on the symmetry and evolution of classical hydrodynamic instabilities [27], or, vice versa, on unraveling the influence of convective flows on bifurcations that occur in already complex chemical systems [28–31]. For example, self-propagating autocatalytic fronts can be periodically deformed by antagonistic solutal and thermal density [32,33] or surface-driven flows [34] in the presence of differential diffusion, by the competition between buoyancy and Marangoni forces [35] or due to
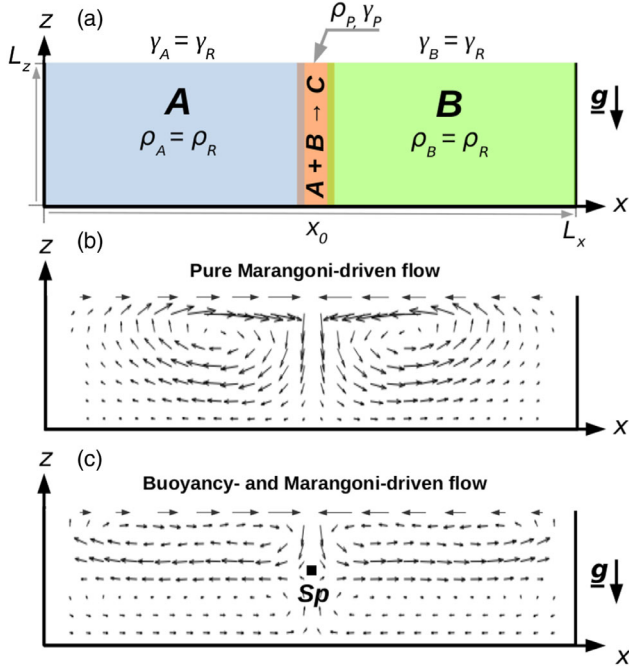
FIG. 1. (a) Sketch of the $A + B \rightarrow C$ configuration used to generate chemohydrodynamic oscillations. The two reactants A and B have the same density ρ_R and surface tension γ_R while the formation of C in the reactive zone can decrease locally the density $\rho_P \leq \rho_R$ and increases the surface tension $\gamma_P > \gamma_R$. Typical initial topology of the chemically induced velocity field (b) in the presence of pure Marangoni flows and (c) when both buoyancy and surface tension forces are antagonistically at play. The black square in panel (c) indicates the stagnation point, Sp.

high surface-tension-driven stresses [36,37]. In the former cases, the autocatalytic nature of the chemical kinetics is crucial to restore, on a proper timescale, a fairly flat interface after deformation and the periodic dynamics is sensitive to the direction of front propagation. In the latter, the wavy structure propagating with the front is a direct consequence of mechanical stresses acting at the quasihorizontal interface between the reacted and nonreacted fluids and relies on very specific chemical reactions.

Differently from previous approaches, we aim at exploiting chemically induced convective feedbacks to design chemohydrodynamic oscillations with the general class of $A + B \rightarrow C$ reactions. The reactive process is nonoscillatory and the related product fuels *in situ* convective motion by inducing a local increase of the surface tension. This flow is not oscillatory either but its combination with the reactive source and diffusion leads to pulsatile emergent behaviors. By including antagonistic buoyancy forces arising from concurrent density changes, we can further sustain and regulate these oscillatory dynamics.

Model.—We consider a two-dimensional isothermal reactor of length L_x and height L_z in a (x, z) reference frame, where the z axis is oriented vertically against the gravitational acceleration $\mathbf{g} = (0, -g)$. The initial spatial

distribution of the chemical species concentrations A, B, C is

$$(A, B, C) = (A_0, 0, 0) \quad \text{for } x < x_0 = L_x/2 \quad \forall z.$$
$$(A, B, C) = (0, B_0, 0) \quad \text{for } x > x_0 \quad \forall z.$$
$$(A, B, C) = (A_0, B_0, 0) \quad \text{for } x = x_0 \quad \forall z.$$

For simplicity, we choose $A_0 = B_0$ and consider the same surface tension, γ_R, and density, ρ_R, for the reactant solutions. Chemical species are also taken with the same diffusivity to ensure a symmetrical development of the reactive zone [15,16,38,39]. The formation of the product C occurs upon diffusive mixing of the two reactants A and B across the initial contact line localized at x_0. C starts diffusing horizontally toward the lateral borders and, in the reactive zone, the medium surface tension locally changes to γ_P ($\gamma_P > \gamma_R$) and the density to ρ_P ($\rho_P \leq \rho_R$) [see Fig. 1(a)], which induces convective transport.

The resulting nonlinear dynamics is governed by a set of partial differential RDC equations (1) and (2) coupled to the incompressible Navier-Stokes equations (3) and (4) via the state equations for the density $\rho = \rho_0(1 + (1/\rho_0)\sum_I I\partial_I\rho)$ and the surface tension $\gamma = \gamma_0(1 + (1/\gamma_0)\sum_I I\partial_I\gamma)$, where $I = A$, B, C are the dimensional concentrations of the chemical species, $(1/\rho_0)\partial_I\rho$ and $(1/\gamma_0)\partial_I\gamma$ are the density and surface tension solutal coefficient of the Ith species, ρ_0 and γ_0 are the solvent density and surface tension, respectively. The dimensionless form of this RDC system, derived in the Boussinesq approximation and written in the ω–ψ form [i.e., using the definitions that relate the velocity field $\mathbf{v} = (u, v)$ to the vorticity $\omega = \nabla \times \mathbf{v}$ and to the stream function, ψ, $u = \partial_z\psi$ and $v = -\partial_x\psi$], reads [19,35]

$$\partial_t a + (\partial_z\psi\partial_x a - \partial_x\psi\partial_z a) = \nabla^2 a - ab, \quad (1)$$

$$\partial_t b + (\partial_z\psi\partial_x b - \partial_x\psi\partial_z b) = \nabla^2 b - ab, \quad (2)$$

$$\partial_t\omega + (\partial_z\psi\partial_x\omega - \partial_x\psi\partial_z\omega) = S_c[\nabla^2\omega - \Delta R(\partial_x a + \partial_x b)] \quad (3)$$

$$\partial_{xx}^2\psi + \partial_{zz}^2\psi = -\omega. \quad (4)$$

Taking into account the conservation of the chemical concentrations: $a + b + 2c = 1 \, \forall x, z, t$, valid when $A_0 = B_0$ and the species diffuse at same rate, we can directly reconstruct the dimensionless concentration field of the product, $c(x, z, t)$. The equation system is casted in dimensionless form by using the RD scales for time, $t_0 = 1/(ka_0)$, length, $L_0 = \sqrt{Dt_0}$, and concentration, A_0 (k is the kinetic rate constant and D the species diffusivity). The Schmidt number $S_c = \mu/D\rho_0 = 1000$ (μ is the dynamic viscosity). $\Delta R = R - R_c/2$, with $R = R_a = R_b$ because the reactant solutions have the same density. $R_i = \partial_I\rho A_0 L_0^3 g/(D\mu)$ is the solutal Rayleigh number of the ith

species and the dimensionless density $\tilde{\rho} = (\rho - \rho_0)/\rho\prime = \Delta R(a + b) + R_c/2$, with $\rho\prime = \mu/(t_0 L_0 g)$. Equations (1)–(4) are solved [40] by using no-flux boundary conditions for the chemical concentrations at the four boundaries of the reactor and no-slip conditions for the velocity field at the three solid boundaries.

To include the shear force at the free surface, we impose at $z = L_z$ the Marangoni boundary condition $\omega = -\Delta M(\partial_x a + \partial_x b)$, where $\Delta M = M - M_c/2$, with $M = M_a = M_b$ as the reactant solutions are considered with the same surface tension. The solutal Marangoni number for the ith species writes $M_i = -1/(\mu\sqrt{kD})\partial_I \gamma$ and the dimensionless surface tension $\tilde{\gamma} = (\gamma - \gamma_0)/\gamma\prime = -\Delta M(a_s + b_s) - M_c/2$ (where $\gamma\prime = \mu L_0/t_0$, and a_s and b_s are the surface concentrations of a and b, respectively). R_c and M_c modify $\tilde{\rho}$ and $\tilde{\gamma}$, respectively, by a constant, while ΔR and ΔM represent the relevant parameters for controlling the onset of oscillations as they tune the relative importance of solutal buoyancy and surface tension contributions to convective flows. Positive ΔR and ΔM mean that the density decreases while the surface tension increases during the reaction.

Chemo-Marangoni-driven oscillations.—We first discuss the minimal case where a chemohydrodynamic oscillatory instability can be obtained with an $A + B \rightarrow C$ reaction, which is in the presence of pure Marangoni-induced convection ($\Delta R = 0$). Figure 2(a) shows the nucleation and development of symmetric waves from the center of the reactor, where C is first formed, toward the lateral borders. Oscillations occur beyond a critical threshold $\Delta M_{\text{crit}} \sim 100$ (slightly changing with L_z).

The complex mechanism of wave formation can be followed in Figs. 2(a) and 2(c) (see also the Supplemental Material [41]): the formation of C locally increases the surface tension at the reaction front, inducing convergent Marangoni flows at the surface and hence a vertical downflow that advects the product toward the rigid bottom boundary. This causes the deformation of its concentration field into two symmetrical fronts (see arrows in snapshots at $t = 50$). The return flow amplifies the extent of these fronts, advects the reactants from one side to the other, feeding a nonlocal reaction zone and sweeping c toward the top of the reactor. This breaks the two initial convective rolls and weakens the vertical convective forcing around x_0. c can thus relax from the reactor bottom upward as a reaction-diffusion front (see arrows in snapshots at $t = 100$). The lateral dissipation of the symmetric waves favors the rebuilt of the vertical downflow at x_0 that opposes to this RD relaxation and restores initial conditions for a novel oscillatory cycle (indicated by arrows in snapshots for $t = 150$). However, in the absence of a feedback mechanism to recreate the acute gradient in surface concentrations, the sharp surface tension gradient sustaining the downflow at x_0 progressively smoothens, dampening oscillations out because of the reactant consumption and species diffusion.
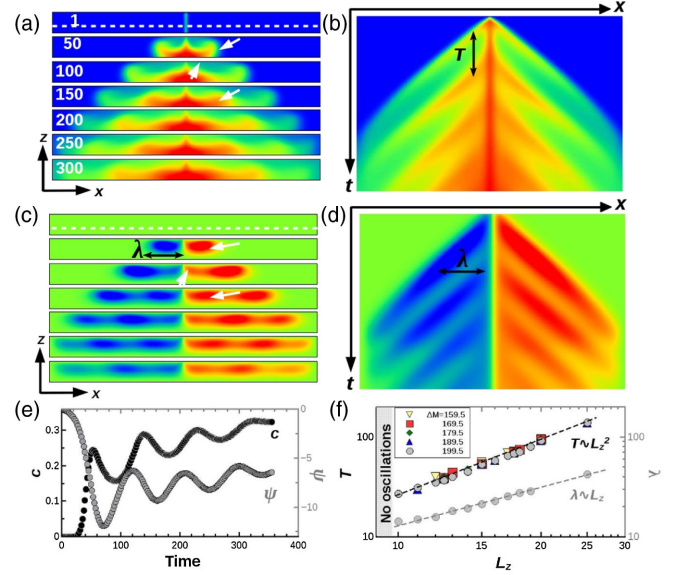
FIG. 2. Chemo-Marangoni-driven oscillations in an $A + B \rightarrow C$ system ($\Delta M = 199.5$, $L_z = 20$). (a),(c) Snapshots of the spatiotemporal evolution of the chemical (c) and hydrodynamic (ψ) fields, respectively, during two typical oscillatory cycles. The arrows at times 50–100–150 indicate in (a) the flow-driven compression relaxation compression of c and in (c) the corresponding hydrodynamic morphology. (b),(d) Space-time plots ($L_x = 256 \times t = 350$) of the dynamics, built along the white line traced in the first snapshot of panels (a) and (c). c ranges between 0 (blue areas) and 0.5 (red areas), while ψ varies between -15 (blue areas) and 15 (red areas). T and λ indicate the characteristic oscillation period and spatial length, respectively. (e) Time series of c (black, left axis) and ψ (gray, right axis) taken at $(x_0 - 20, L_z/2)$. f) Power–law dependence of the oscillation period, T, and the spatial length, λ, on L_z for different ΔM.

The spatiotemporal deployment of these chemo-Marangoni-driven oscillations is illustrated in the space-time plot of Fig. 2(b), where a horizontal concentration profile of c is reported as a function of time. Similarly, the correspondent oscillatory hydrodynamic field is shown in Figs. 2(c) and 2(d), by mapping the evolution of ψ. ψ minima (in blue) and maxima (in red) describe clockwise and counter-clockwise convective rolls, respectively.

To characterize this oscillatory dynamics, we plot the temporal dynamics of c and ψ at a fixed representative point of the reactor. The resulting time series are analyzed to extrapolate the oscillation period, T. The position of ψ minima on the left side (maxima on the right side) and their relative distance are also used to define the spatial characteristic wavelength, λ. T and λ are compared for different values of the control parameters, L_z and ΔM. Though the threshold for spatiotemporal oscillations is critically sensitive on ΔM, both T and λ do not vary significantly with this parameter, as we can see in Fig. 2(f) where the periods for different ΔM collapse to similar values at fixed L_z. On the other hand, increasing ΔM increases the oscillation amplitude (not shown here).

By contrast, the extent of the convective rolls presents a direct correlation with L_z ($\lambda \sim L_z$) that also controls T [Fig. 2(f)]. In particular, the period at which waves are emitted from the center grows by increasing L_z according to $T \sim L_z^2$ and waves formation is suppressed below a critical height $L_c \sim 10$, which slightly shifts to higher values when ΔM decreases. This dependence of the instability threshold on L_z can be inferred from phenomenological arguments. Since waves result from the transverse competition between the Marangoni-driven return flow and the vertical RD relaxation that levels out the local concentration gradients at the surface, the Marangoni timescale τ_{Ma} compatible with the oscillation characteristic length λ has to be smaller than the reaction-diffusion timescale τ_{RD} needed to cover a distance $\mathcal{O}(L_z)$. According to the typical form describing the vertical profile of the horizontal velocity of a Marangoni return flow [36,42], we can assume the characteristic Marangoni velocity to scale as $u_{Ma} \sim \Delta M(\partial_x a_s + \partial_x b_s) L_z$ [where a_s and b_s are considered for $x \to (x_0)^{\pm}$] and $\tau_{Ma} \sim \lambda/|u_{Ma}|$. As $\lambda \sim Lz$ [Fig. 2(f)] and $\tau_{RD} \sim L_z^2$, we find that $L_z > L_c \sim [|\Delta M(\partial_x a_s + \partial_x b_s)|]^{-1/2}$. The layer thickness L_z is thus a determinant parameter that modulates the balance between the reaction-diffusion and the convective timescales. Below L_c the vertical RD process overcomes Marangoni-driven dynamics and kills or even prevents oscillations.

Finally, the spatial width of the system, L_x, affects the oscillatory transient, as oscillations die out sharply when the product front touches the lateral borders. However, the main oscillation properties (T and λ) do not depend on this parameter.

Chemo-Marangoni-buoyancy-driven oscillations.—We next discuss the system dynamics when buoyancy forces are concurrently at play. In particular, we consider the case where the formation of C, by decreasing the local density of the medium, generates an antagonistic vertical upflow opposing the Marangoni-induced flow. The main effect of this buoyancy contribution is to reduce the vertical extent of the domain pertaining Marangoni-related flows [see Fig. 1(c)]. The extent of the competitive buoyancy convective rolls at the reactor bottom depends on the density difference between the reactants and the product, as controlled by ΔR. An illustration of spatiotemporal oscillations in this system is given in Figs. 3(a) and 3(b). The phenomenology is similar to the one described in the pure Marangoni case: surface-tension-triggered downflow is immediately operational upon formation of the product and pushes c toward the bottom. Here, buoyancy forces combine to RD processes to bounce back the local accumulation of the less dense product and, thus, amplify the oscillatory mechanism (see the Supplemental Material [41]). As a consequence, the ψ time series reported in Fig. 3(c) shows an initial growth of the oscillation amplitude. This is different from the pure chemo-Marangoni-driven instability where oscillations dampen out monotonically.
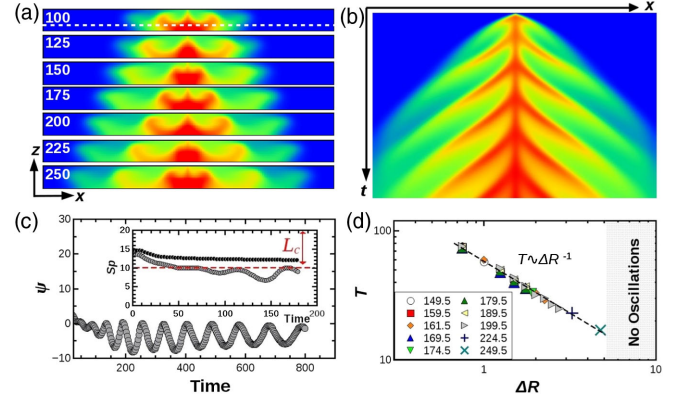
FIG. 3. Chemo-Marangoni-buoyancy-driven oscillations ($\Delta M = 199.5$, $\Delta R = 1.75$, $L_z = 20$). (a) Snapshots of the spatiotemporal evolution of c during two typical oscillatory cycles. (b) Space-time plot ($L_x = 256 \times t = 600$) of the dynamics, built along the white line traced in the first snapshot of panel (a). c ranges between 0 (blue areas) and 0.5 (red areas). (c) Time series of ψ, taken at ($x_0 - 20$, $L_z/2$), for an oscillatory case (gray curve, $\Delta M = 199.5$, $\Delta R = 1.75$, $L_z = 20$). The inset of panel (c) shows the evolution of the stagnation point, Sp, for a typical oscillatory (gray) and a nonoscillatory (black) dynamics (L_c indicates the critical reactor height for the onset of oscillations in the corresponding Marangoni-driven case). (d) Power–law dependence of the oscillation period on ΔR for various $\Delta M \in (149.5, 249.5)$.

Chemo-Marangoni-buoyancy-driven oscillations occur when surface tension forces dominate over buoyancy forces (i.e., for $\Delta R \in [0, 4.75]$ with $\Delta M \geq 149.5$). As such, the spatial extent of the Marangoni-related convective rolls [given by $L_z - Sp$, where Sp is the inversion point of the vertical velocity along the z axis at x_0; see Fig. 1(c)] grows in time, first monotonically, and then undergoes a periodic evolution when oscillatory dynamics start. This behavior can be appreciated in the inset of Fig. 3(c), where Sp is traced as a function of time. Note that the onset of oscillations occurs only when $L_z - Sp > L_c$ (red dashed line), i.e., beyond the critical threshold L_c where the oscillatory instability is also expected in the pure Marangoni case. Conversely, if buoyancy contribution prevails over Marangoni flows (i.e., $\Delta R > 4.75$ and $\Delta M \in [0, 249.5]$), the extent of buoyancy-driven convective rolls grows upward and the vertical residual space to initiate the oscillatory mechanism via surface tension effects falls below L_c, when oscillations cannot start or be maintained [black curves shown in Fig. 3(c)]. Suitable conditions for oscillations span thus the parameter region $\Delta R \in [0, 4.75]$, $\Delta M \in [149.5, 249.5]$ for $L_z \sim 20$.

Consistently with the trend observed in the pure Marangoni-driven scenario, Fig. 3(d) indicates that the characteristic oscillation period decreases by increasing ΔR, as this parameter reduces the spatial domain where the Marangoni-driven convection is effective, like it happens when L_z is decreased in the absence of buoyancy-driven convection. Again, increasing ΔM has a negligible impact on the oscillation period, but it can enhance the oscillation

amplitude by causing a larger vertical displacement of C and a corresponding buoyancy-driven response.

To summarize, we have shown that a simple chemo-hydrodynamic mechanism can sustain spatiotemporal chemical oscillations in an $A + B \rightarrow C$ reaction. This process works in batch conditions, without any external feed or chemical nonlinearity, expanding thereby the realm of chemical oscillations to ubiquitous bimolecular reactions. The trigger for the onset of this oscillatory instability is the hydrodynamic feedback promoted *in situ* by the chemical reaction, that increases the surface tension across the reactive zone, thus promoting a Marangoni convergent flow at the surface and, by continuity, a quasihorizontal return flow into the bulk. The competition between this flow and transversely oriented RD relaxation, that alternately dominate the dynamics, is at the basis of chemo-Marangoni-driven oscillations. Since the reaction-diffusion feedback is weak, oscillations dampen out quickly when only Marangoni convection is at play. The presence of antagonistic buoyancy-driven forces strengthens the upward counterbalance to Marangoni downflow, and the oscillatory mechanism can be either further enhanced leading to chemo-Marangoni-buoyancy-driven oscillations or suppressed, depending on the relative strength of the two contributions to the flow. Since we considered closed reactors, the periodic phenomena presented here are intrinsically transient but oscillations can be stabilized in open conditions with a constant lateral feeding of fresh reactants (see the Supplemental Material [41]). Differently from classical cases where Marangoni stresses can promote oscillatory instability thanks to an externally imposed constant spatial gradient of temperature [42], the periodic phenomenon here is induced *in situ* by a reactive source. The coupling between the chemical reaction and hydrodynamics is thus the essential ingredient for this emergent behavior.

The mechanism discussed above presents a broad interest because the chemical scheme used can be tailored to any second-order process and its simplicity paves the way for an experimental implementation of such a class of oscillators (periodic dynamics were found in self-propelled aspirin boats powered by dissolution-driven Marangoni flows [43]), as well as for devising smart dynamics in reactive flows with applied relevance.

---

*Corresponding author.
mabudroni@uniss.it
†Corresponding author.
lrongy@ulb.ac.be

‡These authors contributed equally to this work.

[1] C. Li, L. Xu, L. Zhu, S. Zou, Q. H. Liu, Z. Wang, and H. Chen, Phys. Rev. Lett. **121**, 104501 (2018).

[2] A. W. Hauser, S. Sundaram, and R. C. Hayward, Phys. Rev. Lett. **121**, 158001 (2018).

[3] I. R. Epstein, K. Kustin, P. De Kepper, M. Orbán, Sci. Am. **248**, 112 (1983).

[4] G. Nicolis and I. Prigogine, *Self-Organization in Non-equilibrium Systems* (Wiley, New York, 1977).

[5] R. Tomasi, J.-M. Noël, A. Zenati, S. Ristori, F. Rossi, V. Cabuil, F. Kanoufi, and A. Abou-Hassan, Chem. Sci. **5**, 1854 (2014).

[6] Z. Zhang and O. Steinbock, Chaos **27**, 093921 (2017).

[7] A. F. Taylor, M. R. Tinsley, F. Wang, Z. Huang, and K. Showalter, Science **323**, 614 (2009).

[8] K. Gizynski and J. Gorecki, Phys. Chem. Chem. Phys. **19**, 28808 (2017).

[9] P. L. Gentili, M. S. Giubila, and B. M. Heron, Chem. Phys. Chem. **18**, 1831 (2017).

[10] M. A. Budroni, S. Garroni, G. Mulas, and M. Rustici, J. Phys. Chem. C **121**, 4891 (2017).

[11] R. Yoshida, Adv. Mater. **22**, 3463 (2010).

[12] N. J. Suematsu, Y. Mori, T. Amemiya, and S. Nakata, J. Phys. Chem. Lett. **7**, 3424 (2016).

[13] A. Isakova and K. Novakovic, J. Mater. Chem. B **6**, 5003 (2018).

[14] I. R. Epstein and K. Showalter, J. Phys. Chem. **100**, 13132 (1996).

[15] L. Gálfi and Z. Rácz, Phys. Rev. A **38**, 3151 (1988).

[16] Z. Jiang and C. Ebner, Phys. Rev. A **42**, 7483 (1990).

[17] A. De Wit, K. Eckert, and S. Kalliadasis, Chaos **22**, 037101 (2012).

[18] C. Almarcha, P. M. J. Trevelyan, P. Grosfils, and A. De Wit, Phys. Rev. Lett. **104**, 044501 (2010).

[19] R. Tiani, A. De Wit, and L. Rongy, Adv. Colloid Interface Sci. **255**, 76 (2018).

[20] S. H. Hejazi, P. M. J. Trevelyan, J. Azaiez, and A. De Wit, J. Fluid Mech. **652**, 501 (2010).

[21] D. Avnir and M. Kagan, Nature (London) **307**, 717 (1984).

[22] V. Loodts, C. Thomas, L. Rongy, and A. De Wit, Phys. Rev. Lett. **113**, 114501 (2014).

[23] S. S. S. Cardoso and J. T. H. Andres, Nat. Commun. **5**, 5743 (2014).

[24] D. Schwabe and A. Scharmann, J. Cryst. Growth **46**, 125 (1979).

[25] J. H. Seinfeld and S. N. Pandis, *Atmospheric Chemistry and Physics* (Wiley & Sons, New York, 2006).

[26] M. Rolle, C. Eberhardt, G. Chiogna, O. A. Cirpka, and P. Grathwohl, J. Contam. Hydrol. **110**, 130 (2009).

[27] L. Lemaigre, M. A. Budroni, L. A. Riolfo, P. Grosfils, and A. De Wit, Phys. Fluids **25**, 014103 (2013).

[28] V. Pérez-Villar, A. P. Muñuzuri, M. N. Lorenzo, and V. Pérez-Muñuzuri, Phys. Rev. E **66**, 036309 (2002).

[29] M. A. Budroni, M. Masia, M. Rustici, N. Marchettini, V. Volpert, and P. C. Cresto, J. Chem. Phys. **128**, 111102 (2008).

[30] F. Rossi, M. A. Budroni, N. Marchettini, and J. Carballido-Landeira, Chaos **22**, 037109 (2012).

[31] M. A. Budroni and A. De Wit, Chaos **27**, 104617 (2017).

[32] L. Rongy, G. Schuszter, Z. Sinkó, T. Tóth, D. Horváth, A. Tóth, and A. De Wit, Chaos **19**, 023110 (2009).

[33] L. Rongy and A. De Wit, J. Chem. Phys. **131,** 184701 (2009).

[34] L. Rongy, P. Assemat, and A. De Wit, Chaos **22,** 037106 (2012).

[35] M. A. Budroni, L. Rongy, and A. De Wit, Phys. Chem. Chem. Phys. **14,** 14619 (2012).

[36] L. Rongy and A. De Wit, J. Chem. Phys. **124,** 164705 (2006).

[37] L. Rongy and A. De Wit, Phys. Rev. E **77,** 046310 (2008).

[38] L. Rongy, P. M. J. Trevelyan, and A. De Wit, Phys. Rev. Lett. **101,** 084503 (2008).

[39] R. Tiani and L. Rongy, J. Chem. Phys. **145,** 124701 (2016).

[40] RDC equations are solved numerically by means of an implicit finite difference method, the alternating direction implicit) method. Typical simulations are run over a spatial domain $L_x = 256 \times L_z = 20$, with the integration space steps $h_x = h_z = 0.25$ and time step $h_t = 10^{-4}$.

[41] See Supplemental Material at http://link.aps.org/supplemental/10.1103/PhysRevLett.122.244502 for movies of the spatio-temporal evolution of the chemohydrodynamic waves shown in Figs. 2 and 3 and the time series of the corresponding open systems.

[42] M. K. Smith and S. H. Davis, J. Fluid Mech. **132,** 119 (1983).

[43] T. Bánsági, M. M. Wrobel, S. K. Scott, and A. F. Taylor, J. Phys. Chem. B **117,** 13572 (2013).